Heliyon 10 (2024) e26844

Contents lists available at ScienceDirect

Heliyon

journal homepage: www.cell.com/heliyon

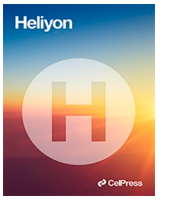

Review article

A review of mesoscopic modeling and constitutive equations of particle-reinforced metals matrix composites based on finite element method

Jing Li [a], Fei Wang [a,b,*], Ce Zhang [a], Qifei Li [a], Tao Chen [c]

[a] School of Mechanical Engineering, Qilu University of Technology (Shandong Academy of Sciences), Jinan 250353, China
[b] Shandong Institute of Mechanical Design and Research, Jinan 250031, China
[c] Shandong Youjiang Intelligent Equipment Co., Ltd, Rizhao, 276500, China

ARTICLE INFO

Keywords:
Mesoscopic structure
Strengthening mechanism
RVE model
Constitutive equation
Interface module

ABSTRACT

Particle reinforced metal matrix composite (PRMMCs) has a complex mesoscopic structure, and the addition of particles can strengthen the metal matrix, which makes the deformation and failure behavior of PRMMCs under load very complicated. The finite element method can quantitatively describe the effect of PRMMCs microstructure parameters on the macroscopic properties of materials, but the key is to establish a representative volume element(RVE) model that can reflect the real mechanical properties of materials. This paper reports and discusses on the construction methods of the RVE model of PRMMCs from three aspects: the geometric modeling of PRMMCs microstructure, the construction of the matrix constitutive equation based on PRMMCs reinforcement mechanism and the interface module. In the end, Abaqus and some of its secondary development functions are introduced.

1. Introduction

Particle reinforced metal matrix composites (PRMMCs) have high specific strength, modulus and thermal conductivity, low expansion properties, and excellent wear resistance and designability, showing great application potential in aerospace, transportation, energy and the environment [1–3].

PRMMCs are materials formed by dispersing reinforcing particles (such as B_4C, SiC, Al_2O_3, etc.) into the metal matrix [4]. The PRMMCs exhibits an intricate mesoscopic architecture, featuring a non-uniform and chaotic arrangement of particles. The incorporation of particles can further enhance the properties of metal matrix. These characteristics make the deformation and failure behavior of PRMMCs under load very complicated [4–6]. The finite element analysis enables a quantitative description of the influence of PRMMC microstructure parameters on the macroscopic properties of materials, thereby directly revealing the interplay between the reinforcement phase, interface phase, and macroscopic mechanical properties [7], which is an efficient method to study the mechanical properties of PRMMCs.

By studying the relationship between mechanical properties and mesoscopic structure of PRMMCs with the finite element method, the design, preparation and processing technology of PRMMCs can be optimized to meet the requirements of industrial design and

* Corresponding author. School of Mechanical Engineering, Qilu University of Technology (Shandong Academy of Sciences), Jinan 250353, China.
E-mail address: wf@qlu.edu.cn (F. Wang).

https://doi.org/10.1016/j.heliyon.2024.e26844
Received 26 September 2023; Received in revised form 14 February 2024; Accepted 20 February 2024
Available online 23 February 2024

application [4,7]. For instance, the application of materials is inseparable from mechanical processing, which typically involves precise cutting. The quality of the machined surface constitutes a crucial factor that impacts the actual properties of the material [8]. With the help of finite element simulation, the cutting model of PRMMCs can be established, and the stress-strain relationship, damage form and dynamic chip formation mechanism inside the material during cutting can be simulated from a microscopic perspective [9,10], so as to optimize the processing technology and improve the processing quality.

To use finite element simulation, the finite element model must be established first. The finite element model of PRMMCs can be divided into macroscopic model and mesoscopic model from spatial scale. In the macroscopic model, PRMMCs is regarded as a homogeneous material, and the equivalent mechanical properties of the material are mainly considered, such as Young's modulus, Poisson's ratio, yield strength, ultimate tensile strength, etc [11]. The mesoscopic model starts with the mesoscopic structure of PRMMCs, comprehensively considers the volume fraction, shape, size and distribution of particles, and separately considers the mechanical properties of each component [11–15], and establishes the representative volume element(RVE) model of PRMMCs [11].

In this paper, the modeling method of RVE model of PRMMCs is studied. The modeling method of PRMMCs mesoscopic geometric model is summarized. The constitutive equation of metal matrix is introduced in detail, including a deep discussion on the strengthening mechanism of PRMMCs. The interface model and the method of obtaining performance parameters are summarized. In the end, Abaqus and some of its secondary development functions are introduced.

2. Methods of geometric modeling

PRMMCs has a complex microstructure, and the construction of its geometric model is a difficult problem in finite element method. This part mainly starts with the construction of PRMMCs mesoscopic structure model, and summarizes the previous modeling methods.

2.1. Simplified model

In order to quickly build the model, scholars simplified the mesostructure of PRMMCs, simplified the reinforcement particles into circles or spheres, and arranged them regularly to establish two-dimensional(2D) and three-dimensional(3D) geometric models of PRMMCs [16–18]. The current modeling method, however, fails to account for the influence of particle shape and distribution, resulting in significant deviations between simulation results and actual outcomes. In certain studies that overlook the shape and distribution of the reinforcement phase, such as investigating the impact of tool position changes on machining and interface phase destruction behavior, enhancing simulation efficiency can be achieved [18–20].

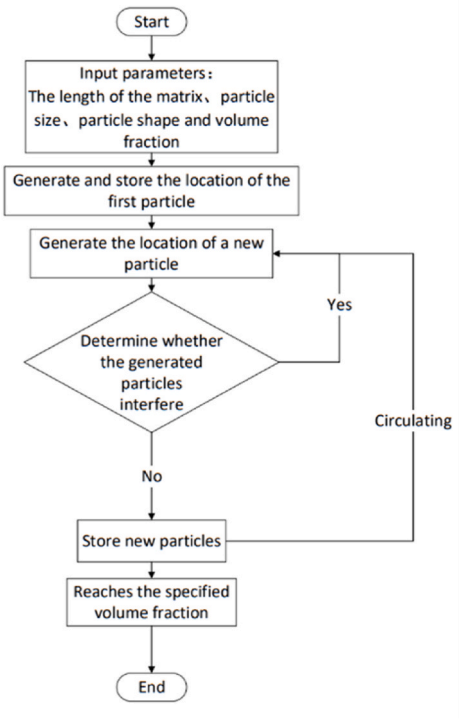

Fig. 1. Flowchart of RSA

2.2. Computer parametric modeling

When the influence of the particle shape of the reinforcement is not considered, the particles are simplified into regular geometry, and a script is written to randomly insert the particles with the help of stochastic algorithm [21–23], or the geometric model of PRMMCs is generated with the help of Digimat software [24]. Non-interference and random distribution of particles is the key to stochastic algorithm [5]. The stochastic algorithm proposed earlier is called Random Sequential Adsorption(RSA), and its process is shown in Fig. 1[25].

However, the method of RSA is difficult to add new particles after the particles reach a certain volume fraction, so that the model with higher particle volume fraction cannot be generated by this algorithm [26]. Since then, some scholars have continuously improved the stochastic algorithm, proposing the nearest neighbor algorithm (NNA) [27,28], the random sequence extension (RSE) [29] and the discrete element method (DEM) [30]. Miao et al. [31] proposed a method to avoid particle overlap by using the collision mechanism of rigid particles.

In order to generate reinforcement particles with irregular shape, different methods have been proposed by different scholars. Chen [32] generates random convex polyhedra by extension of regular polyhedra. Su [33] and Wu [34] generated convex polyhedra by stretching two-dimensional graphs and then cutting edges, as shown in Fig. 2.

Wang [35] comprehensively considered the uneven structure of the particle surface and generated random polyhedra by writing scripts in Python language. First, a regular polyhedron is generated and each vertex of the polyhedron is numbered, as shown in Fig. 3 (a); Then polar coordinates are established with the center of the regular polyhedron as the origin, and each vertex of the polyhedron can be represented by radius r_n, azimuth θ_n and elevation φ_n. By transforming these three parameters according to Equation (1), a random polyhedron with uneven structure can be obtained, as shown in Fig. 3(b); The irregular particles obtained are depicted in Fig. 3 (c). The $random(-1,1)$ indicates that a random number is taken between -1 and 1.

$$\begin{cases} r_n = r_{n0} + d_r \cdot random(-1,1), d_r \in \left(-\dfrac{D}{2}, \dfrac{D}{2}\right) \\ \theta_n = \theta_{n0} + d_\theta \cdot random(-1,1), d_\theta \in (-22.5^\circ, 22.5^\circ) \\ \varphi_n = \varphi_{n0} + d_\varphi \cdot random(-1,1), d_\varphi \in (-22.5^\circ, 22.5^\circ) \end{cases} \tag{1}$$

With the help of computer parametric modeling, meso-geometric models with different structures can be generated by adjusting the parameters of the model, such as Fig. 4 (a) and (b). For example, in Wang [35] 's method, by changing the radius of nodes at different positions, the aspect ratio of the generated particles can be controlled, and the morphology of the particles can be changed by adjusting the number of nodes and the transition factor. Therefore, this modeling method has strong universality. However, this modeling method uses a random way to generate the microstructure (particle distribution and morphology) of PRMMCs, which is still different from the actual situation.

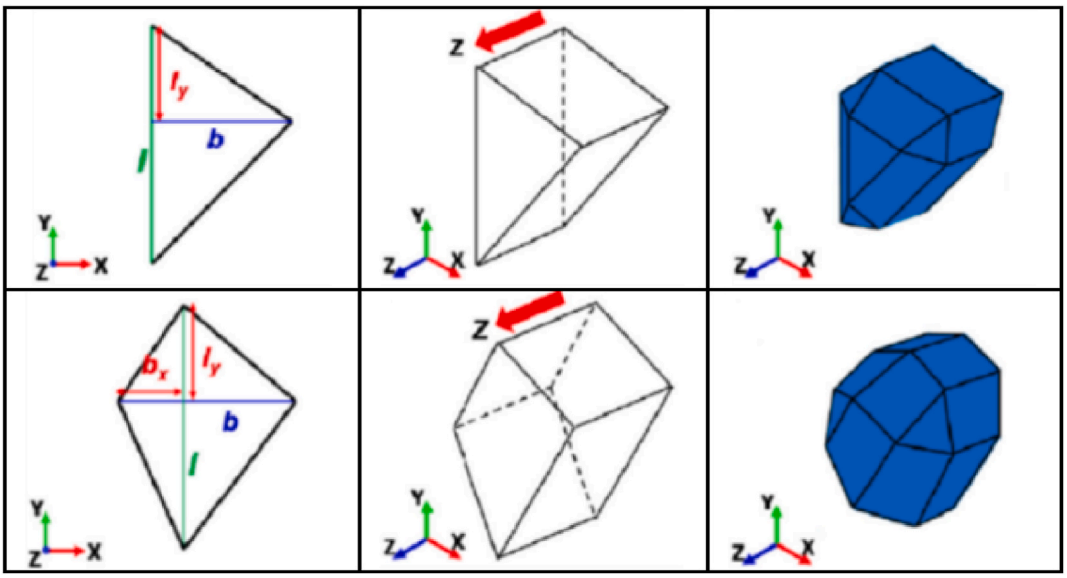

Fig. 2. Stretching a plane to form a polyhedron.

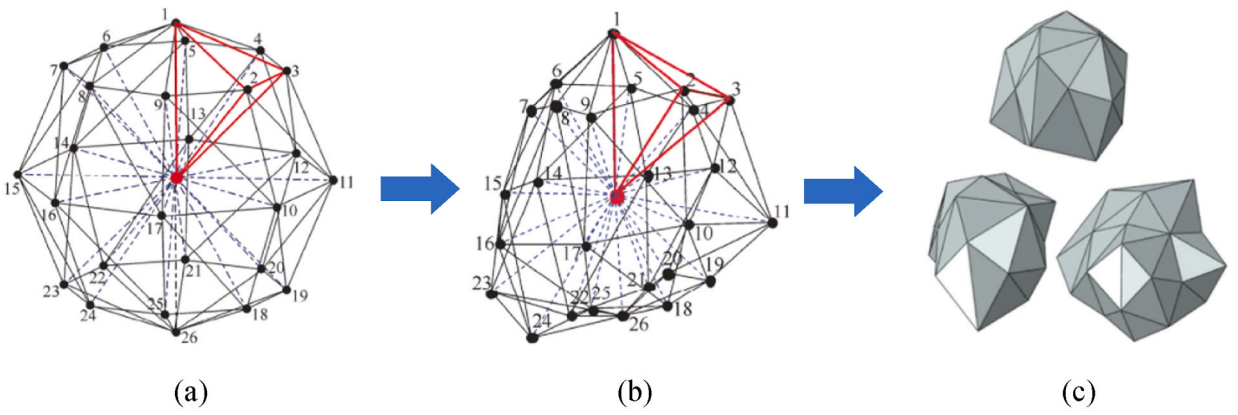

Fig. 3. Generating irregular polyhedra with the help of node waves (a) regular polyhedron (b) random polyhedron (c) irregular particles.

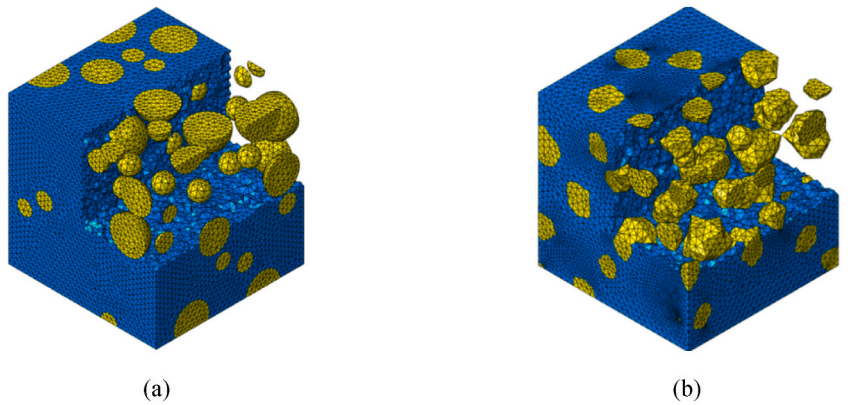

Fig. 4. Parameterized modeling generated PRMMCs RVE models (a) spherical particles (b) irregular polyhedral particles.

2.3. The real structure model

Scanning electron microscope (SEM) or optical microscope was used to obtain the microscopic images of PRMMCs, and a series of image processing software was used to extract the microscopic features in the images to obtain the two-dimensional(2D) true structure model of PRMMCs, as shown in Fig. 5 [6,36].

Xiang [36] mapped the pixel dots of the picture into the finite element mesh in the simulation model by processing the real structure picture, and adjusted the size of the image pixels to achieve the density of the mesh, as shown in Fig. 6. This method can guarantee the quality of finite element mesh, thus improving the precision and efficiency of finite element calculation.

The 2D real structure method can restore the mesoscopic characteristics of PRMMCs, and the mesoscopic structure model of materials can be generated with the help of corresponding equipment and software, which is a convenient finite element modeling method. However, this model is limited to the analysis of two-dimensional stress-strain behavior in PRMMCs, whereas practical problems often involve three-dimensional complexities. Therefore, it is imperative to construct a three-dimensional (3D) realistic structural model for particle-reinforced composites.

X-ray tomography (X-CT) [37], based on the principle that different components of materials have different radiation-resistance rates to X-rays, can obtain the structure of the object through computer processing of the collected data, and stack the 2D images to form a 3D structure model.

Peng et al. [14] generated a 3D model of B_4C_p/Al through X-CT technology, as shown in Fig. 7.

This method can effectively take into account the distribution of particles in PRMMCs, but limited by the resolution of X-CT, some of the micro-nano reinforcement particles with sharp angular structure may be lost.

On the basis of the 2D real structure method, the material is continuously sliced and polished to obtain a series of microstructure photos. With the help of computer software, these two-dimensional pictures are sequentially superimposed to form a 3D model of the material, as shown in Fig. 8[38], which is called the serial sectioning method here.

N. CHAWLA et al. [39] earlier applied this method to the finite element simulation of PRMMCs, and compared it with the simplified model (spherical and ellipsoidal reinforcement particles), as shown in Fig. 9 (a) to (c). The results show that the model established by the serial sectioning method has higher accuracy than the simplified model.

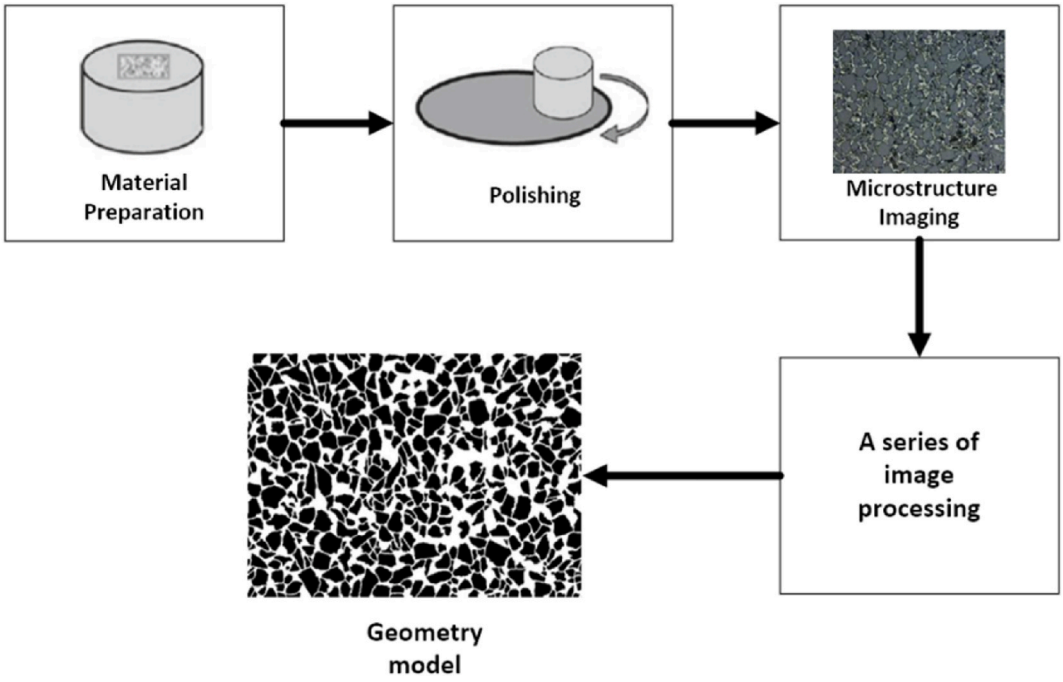

Fig. 5. The process of the 2D real structure method.

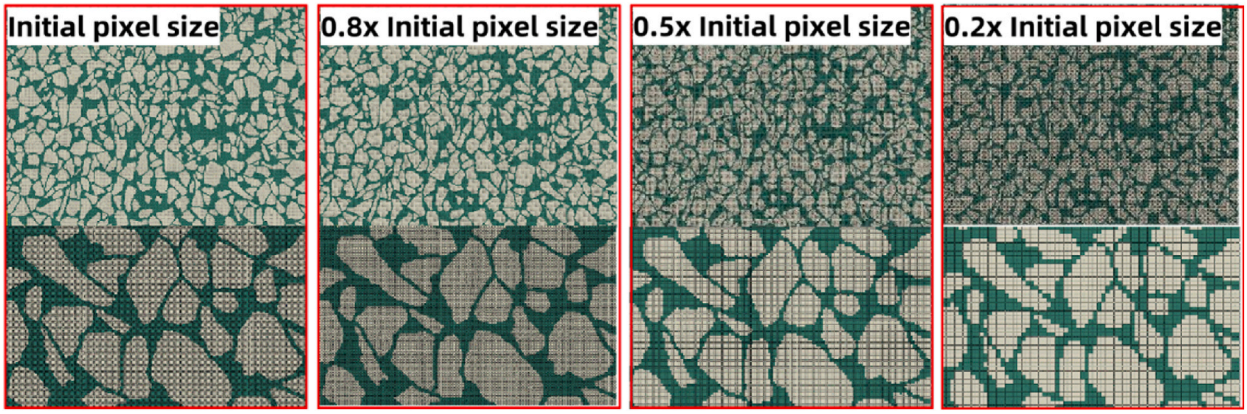

Fig. 6. RVE models with different mesh sizes.

The 3D true mesoscopic structure model of PRMMCs can be obtained by serial sectioning method, but this method requires continuous grinding and image processing of the sample, which consumes a lot of time and cannot preserve the integrity of the sample.

3. Research on the constitutive models of materials

Under the action of load, the material is affected by large strain, strain rate and high temperature. Under the influence of strain hardening and heat softening, the stress and other parameters of the material in the deformation process change dynamically. In order to describe this dynamic behavior of the material, a mathematical equation linking the stress, strain rate, strain rate and time is needed, it is called the constitutive equation [40]. A constitutive equation that accurately describes the material's mechanical properties is crucial for finite element simulation.

For a long time, in order to describe the mechanical properties of materials more accurately, a large number of constitutive equations have been proposed. Currently, the constitutive equations that are widely used include the Johnson-Cook (J-C) model [41] and its improved versions [42–44], the Zerilli-Armstrong (Z-A) model [42], the Maewake model [45], the Nemat-Nasser model [46], and the Power-Law model [47]. Among them, J-C models are frequently used in the simulation of large deformation of metal materials.

The particles of PRMMCs are generally brittle materials, and the JH series (JH1, JH2 [48], and JHB[49] proposed by Johnson and

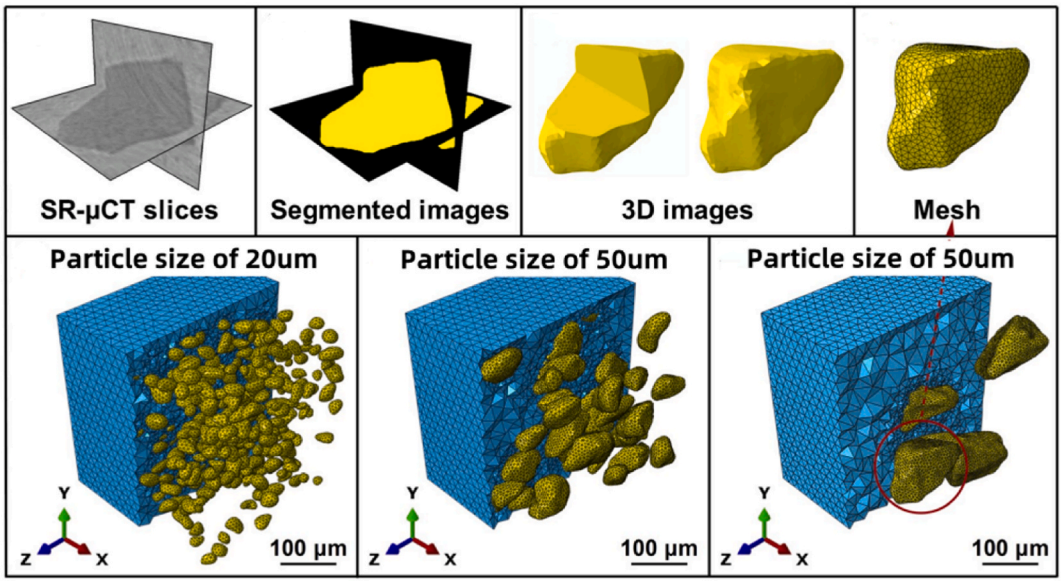

Fig. 7. The 3D RVE model of PRMMCs generated by X-CT.

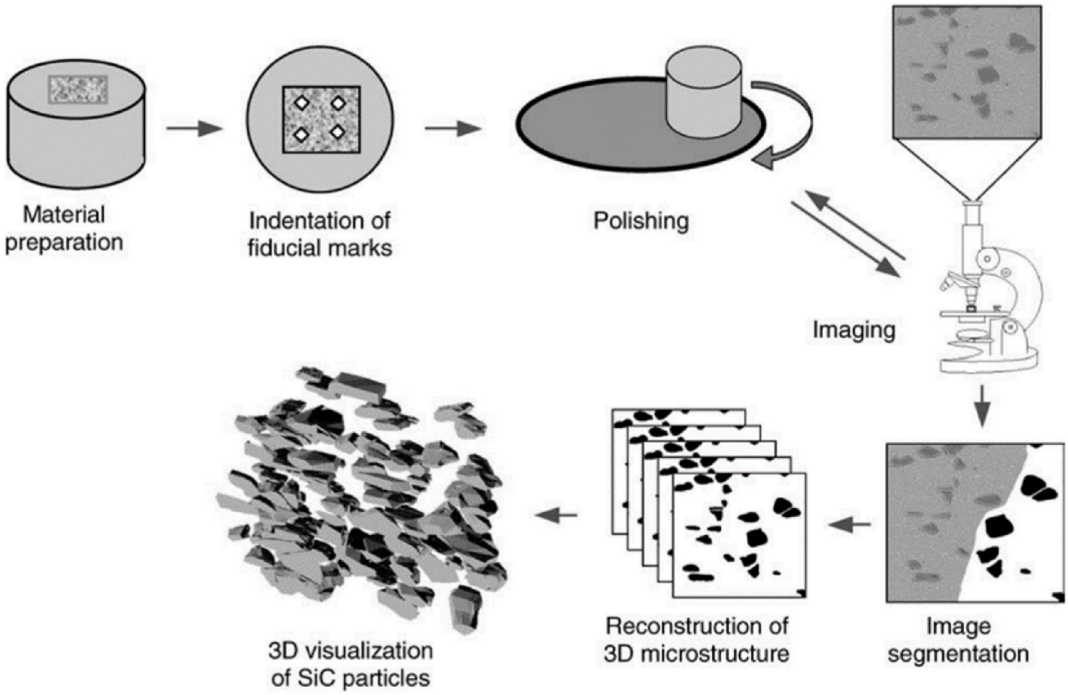

Fig. 8. The process of serial sectioning.

Holmquist are currently widely employed constitutive models for describing the dynamic mechanical behavior of brittle materials. Although there are some difficulties in obtaining parameters for the JH equation, it is still widely used [50–53].

3.1. Reinforcement mechanism of PRMMCs

The reason why PRMMCs have higher strength and stiffness compared to pure metal materials is due to the introduction of reinforcing particles that generate different strengthening mechanisms. The deep comprehension of the strengthening mechanism is essential for enhancing the predictive accuracy of mechanical properties in PRMMCs [54].

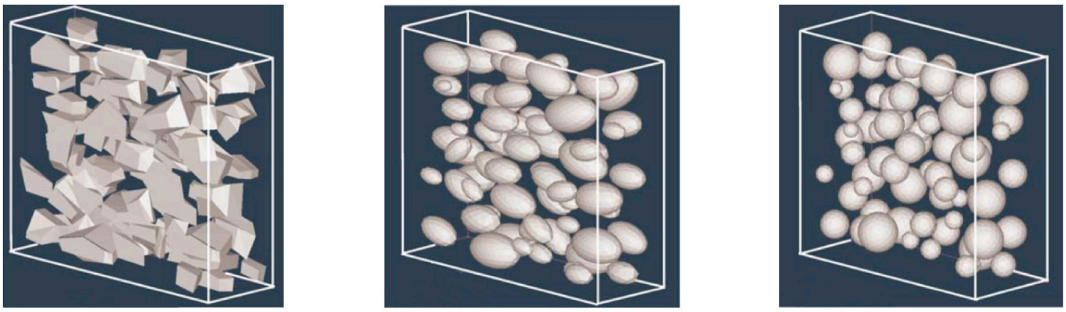

Fig. 9. (a) Real structure model (b) Ellipsoid model (c) Sphere model [34].

The incorporation of high-strength and high-modulus reinforcement particles to directly bear the load transmitted by the matrix is referred to as particle-bearing strengthening [55]. The enhancement effect can be expressed as a function of the particle volume fraction f, this is shown in Equation [2,56].

$$\Delta\sigma_{load} = 0.5f\sigma_m \tag{2}$$

σ_m represents the strength of the un-reinforced metal matrix. A detailed introduction to this strengthening mechanism will not be provided here.

Dislocation strengthening is caused by the intercrossing of dislocations in the metal matrix, which hinders the movement of slip dislocations. The strengthening formula is shown as Equation (3)[57], where ρ is the matrix dislocation density, α_D is the dislocation strengthening coefficient, and G_m and b_m are the matrix shear modulus and the Burgers vector.

$$\Delta\sigma_D = \alpha_D G_m b_m \rho^{\frac{1}{2}} \tag{3}$$

When not subjected to external loads, the dislocation of the PRMMCs matrix is mainly composed of two parts. One part is the dislocations within the lattice that are unrelated to the reinforcing particles, with a lower dislocation density and thus causing little strengthening stress. The other part is the increase in dislocation density caused by the difference in thermal expansion coefficient between the reinforcing particles and the metal matrix (thermal mismatch) during the preparation of the composite material [58]. The calculation formula for the increase is shown in Equation (4), where $\Delta\alpha$ is the difference between the coefficient of thermal expansion of the matrix and the enhanced phase, ΔT is the difference between the preparation temperature and the experimental temperature of the material, and d_p is the particle diameter [55].

$$\rho_{GNDs}^{CTE} = 6\frac{\Delta\alpha\Delta Tf}{b_m d_p(1-f)} \tag{4}$$

The introduction of reinforcing particles will cause grain refinement of the matrix [59]. The smaller the grain size, the greater the volume fraction of grain boundaries, and the more obvious the hindrance to dislocation movement, known as grain boundary strengthening. During the thermal deformation process of the composite material, reinforcing particles with diameters greater than 1 μm can promote the refinement of the matrix grain size. The relationship between the grain diameter D and the reinforcing particle diameter d_p as well as the volume fraction f is shown in Equation (5) [60].

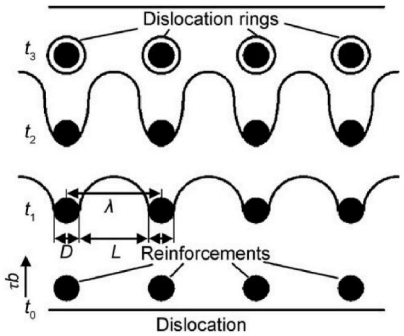

Fig. 10. Schematic diagram of dislocation bypassing through reinforcement particles [62].

$$D = d_p\left[\frac{(1-f)}{f}\right]^{\frac{1}{3}} \tag{5}$$

Hall-Petch is used to describe the strength increment produced by grain refinement, as shown in Equation (6)[61], where K_y is the Hall-Petch coefficient.

$$\Delta\sigma_{H-P} = K_y D^{-\frac{1}{2}} \tag{6}$$

In the deformation process of PRMMCs under load, slip dislocation occurs. When the slip dislocation is blocked by the particle, a bowing equilibrium is formed under external load. When the external load increases further, the slip dislocation passes through the particle in a detour manner, leaving dislocation loops around the particle to hinder dislocation movement [62], as shown in Fig. 10. This phenomenon mainly occurs when the particle diameter is below 1 μm [63], because, in the system of micrometer-sized reinforcements, larger particle spacing cannot form effective dislocation loops. This concept was proposed by Orowan in 1948 and is called Orowan strengthening [64].

The Orowan strengthening is shown as Equation (7)[65], where r_0 is the dislocation core radius, v is Poisson's ratio, η is a constant related to the distribution state of the particles, D and L are related to the shape of the reinforcing phase. M is the Taylor factor.

$$\Delta\sigma_{Orowan} = \frac{\eta M}{2\pi\sqrt{1-v}}\frac{G_m b_m}{L}\ln\left(\frac{\left(D^{-1}+L^{-1}\right)^{-1}}{r_0}\right) \tag{7}$$

The elastic modulus of PRMMCs matrix and particle is different(modulus mismatch), when the material is subjected to external loads, the metal matrix and the reinforcement particles undergo non-uniform deformation, resulting in deformation gradients in the metal matrix, which form geometrically necessary dislocations and cause flow strengthening of the matrix [66,67], as shown in Fig. 11.

The strength increment of the matrix caused by the geometric necessary dislocations is shown in Equation (8)(55).

$$\Delta\sigma_{EM} = \sqrt{3}\alpha G_m b_m\sqrt{\rho_{GNDs}^{EM}} \tag{8}$$

In the formula, α is a constant, usually taken as 0.5, and ρ_{GNDs}^{EM} is the dislocation density caused by modulus mismatch, as shown in Equation (9)(55).

$$\rho_{GNDs}^{EM} = \frac{6f}{b_m d_p}\varepsilon_p \tag{9}$$

Zhang, Andrä et al. [54] comprehensively considered load transfer, thermal residual stress, plastic strain gradient and grain refinement, and established a micro-scale finite element model of PRMMCs to evaluate each strengthening mechanism. The conclusion is as follows.

(1) The main strengthening mechanism of PRMMCs is that particles directly bear the load transmitted by the matrix.
(2) Thermal residual stress affects the yield strength of PRMMCs, but has little effect on the hardening rate after yielding.
(3) Grain refinement increases the yield strength of PRMMCs, and gradient strengthening mainly increases the hardening rate.

3.2. Constitutive models based on strengthening mechanisms

According to the research in Section 3.1, it can be found that the introduction of reinforcement particles with high modulus and high strength will directly or indirectly strengthen the metal matrix. Therefore, the traditional constitutive equation used to describe pure metals will cause large errors in PRMMCs finite element simulation, so it is necessary to develop a constitutive equation to describe the metal matrix based on the micro-strengthening mechanism of composite materials.

The influence of thermal mismatch and modulus mismatch was comprehensively considered by Xiang[36], who integrated multiple strengthening mechanisms and established the constitutive equation of aluminum matrix in SiC_p/Al, as depicted in Equation

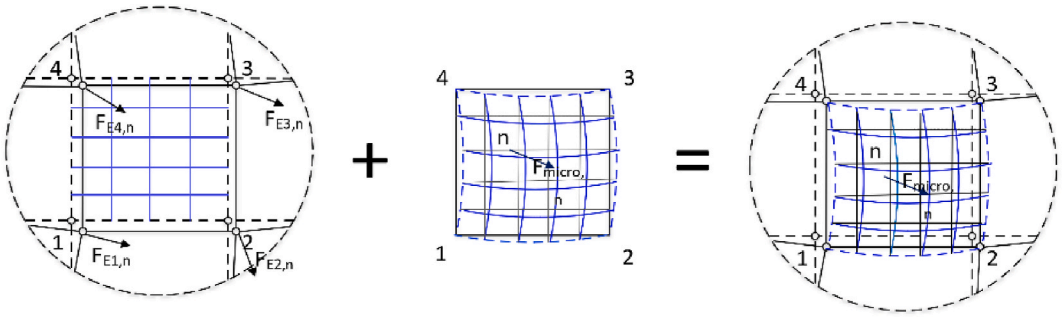

Fig. 11. Non-coherent plastic deformation and strain gradient at the interface [31].

(10)–(12).

$$\sigma_{flow} = \sqrt{\left[\sigma_{ref}f\left(\varepsilon_p\right) + \Delta\sigma_{GNDs}^{CTE}\right]^2 + 6M^2\alpha^2 G_m{}^2 f\frac{b_m}{d_p}\varepsilon_p} \tag{10}$$

$$\sigma_{ref}f\left(\varepsilon_p\right) = \left(A + B\varepsilon^n\right)\left[1 + C\ln\left(\frac{\dot{\varepsilon}}{\dot{\varepsilon}_0}\right)\right]\left[1 - \left(\frac{T - T_0}{T_{melt} - T_0}\right)^m\right] \tag{11}$$

$$\Delta\sigma_{GNDs}^{CTE} = M\alpha G_m b_m\sqrt{\rho_{GNDs}^{CTE}} \tag{12}$$

Where M is the Taylor factor, α is the empirical constant, and ε_p is the plastic strain. Equation (11) is the J-C constitutive equation, which is used here to describe the stress of the unstrengthened aluminum matrix.

Peng et al. [14], considering the influence of thermal mismatch and grain refinement, linearly add the yield strength σ_{Al} of the unstrengthened matrix, the strength increment $\Delta\sigma_{GNDs}^{CTE}$ of the dislocation strengthening and the strength increment $\Delta\sigma_{H-P}$ of the grain refinement, and then coupling with the flow strengthening to obtain the flow stress equation of the aluminum matrix in B_4C_p/Al. As shown in Equation (13)–(15).

$$\sigma_{flow} = \sqrt{\sigma_{m\,,\,y}{}^2 + 27\sqrt{10}\alpha^2 G_m{}^2\frac{b_m}{d_p}f^{\frac{1}{3}}\varepsilon_p} \tag{13}$$

$$\sigma_{m\,,\,y} = \sigma_{Al} + \Delta\sigma_{GNDs}^{CTE} + \Delta\sigma_{H-P} \tag{14}$$

$$\Delta\sigma_{H-P} = K_y d_p{}^{-\frac{1}{2}}\left[\frac{(1-f)}{f}\right]^{-\frac{1}{6}} \tag{15}$$

Equation (15) represents the strengthening contribution caused by grain refinement, where the K_y constant for the aluminum matrix is taken as 0.1 $M/N^{2/3}$.

Ma et al. [68] considered the effects of thermal mismatch and established the constitutive equation for the aluminum matrix in PRMMCs, as shown in Equation (16), and Equation (17) represents the strength of the unreinforced aluminum matrix.

$$\sigma_{flow} = \sqrt{\left[\sigma_{Al}\left(1 + \frac{E_m\varepsilon^p}{\sigma_{Al}}\right)^N + \Delta\sigma_{GND}^{CTE}\right]^2 + 27\sqrt{\frac{5}{2}}\beta^2 G_m\frac{b_m}{r_p}f^{\frac{1}{3}}\varepsilon^p} \tag{16}$$

$$\sigma_{ref}f\left(\varepsilon_p\right) = \sigma_{Al}\left(1 + \frac{E_m\varepsilon^p}{\sigma_{Al}}\right)^N \tag{17}$$

Xiang [36] and Ma [68] both based their research on the dislocation punching mechanism proposed by Taya and Shoichi Shibata [69], considering the distance of the punching zone and calculating the increase in dislocation density in the punching zone to obtain the strength increment caused by the thermal mismatch. The dislocation punching mechanism is shown in Fig. 12 (a) and (b), and the calculation formula based on the punching distance $\overline{R}$ is given by Equations (18)–(20).

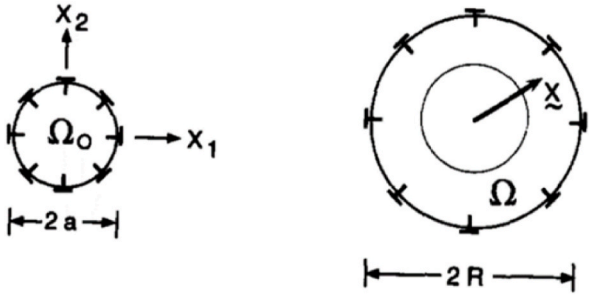

Fig. 12. Schematic diagram of dislocation punching (a) before punching (b) after punching.

$$\overline{R} = r_p \left(\frac{B(1-2Pf) + \sqrt{B^2(1-2Pf)^2 + 16\left(\frac{k}{G_m}\right)PB}}{4\left(\frac{k}{G_m}\right)} \right)^{\frac{1}{3}} \tag{18}$$

$$B = \frac{(1+v_m)|\alpha^*|}{1-v_m} \tag{19}$$

$$P = \frac{2(1-2v_m)(3\overline{\lambda}+2\overline{G})}{(1-v_m)\left[(1-f)(3\overline{\lambda}+2\overline{G})\left(\frac{1+v_m}{1-v_m}\right)+3\left\{f\left(3\lambda_p+2G_p\right)+(1-f)(3\lambda_m+2G_m)\right\}\right]} \tag{20}$$

The subscript " m" and " p" represent the matrix and reinforcing particles. α^* is the product of the difference between the coefficient of thermal expansion of the reinforcement and the matrix and the temperature difference of the material preparation, and $\overline{\lambda} = \lambda_p - \lambda_m$; $\overline{G} = G_p - G_m$. The calculation formula for the dislocation density based on the stamping distance $\overline{R}$ is shown in Equation (21)(31, 65).

$$\rho_{GNDs}^{CTE} = \frac{6\sqrt{2}\Delta CTE \bullet \Delta T \bullet {r_p}^2}{b_m\left(\overline{R}^3 - {r_p}^3\right)} \tag{21}$$

The Taylor non-local plastic theory (TNT) [70] connects the flow strengthening of PRMMCs metal matrix with the statistical storage strengthening to obtain the flow stress equation of the metal matrix, which takes into account the density increase of the geometric must dislocation caused by the modulus mismatch related to the particle size of the reinforced phase, as shown in Equation (22).

$$\sigma_{flow} = \sqrt{\left[\sigma_{ref} f\left(\varepsilon_p\right)\right]^2 + 27\sqrt{\frac{5}{2}}\beta^2 {G_m}^2 \frac{b_m}{r_p} f^{\frac{1}{3}} \varepsilon^p} \tag{22}$$

In the equation, $\sigma_{ref} f(\varepsilon_p)$ represents the statistical storage strength. Taylor non-local plasticity theory has been applied in the above studies [14,36,68].

4. The interface of PRMMCs

As an important component of composite materials, in physical terms, interface refers to the bonding part between the matrix and the particles. Due to the complex shape of the reinforcement phase, the interface is not an ideal flat or curved surface. The components of the matrix phase and the reinforcement phase are combined to form a small transition region with complex mechanical behavior. Based on previous research [54,55], particles are responsible for directly bearing the load transmitted by the matrix and play a primary role in strengthening PRMMCs. The interface of the PRMMCs is responsible for transferring stress [71,72]. The interface failure is manifested as interface debonding, which will lose the load transfer ability. Therefore, the interface strength directly affects the overall strength of the composite [73,74].

4.1. Models of interface

The mechanical model of the interfacial phase is developed based on the mechanics of interfacial fracture. It is divided into two parts: linear elastic fracture mechanics and elastic-plastic fracture mechanics, mainly studying the stress field and strain field at the crack tip, as well as the conditions and laws of crack propagation [75]. According to the stress state near the crack tip, the fracture types are divided into three types: opening, sliding, and tearing, as shown in Fig. 13 (a) to (c). Any form of fracture is a superposition of these

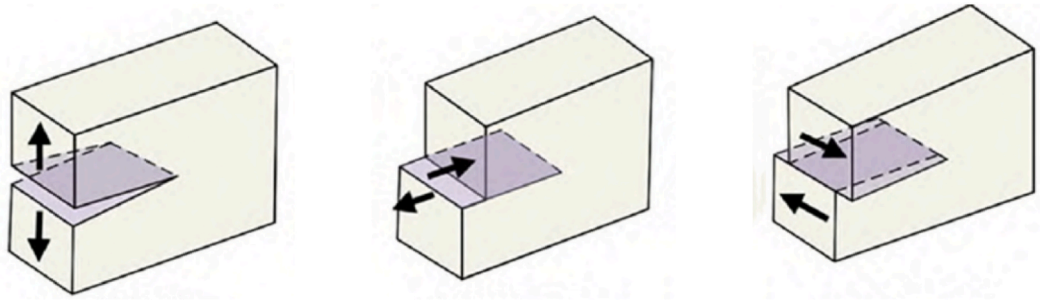

Fig. 13. Three basic fracture modes: (a) opening mode, (b) sliding mode, and (c) tearing mode [75].

three fracture types. Using this method to simulate the generation of interface cracks will produce strong stress singularities, which makes the calculation difficult to converge and has a large error [7,75].

Afterward, G.I. Barenblatt [76] proposed a "cohesive model" based on elastoplastic fracture mechanics, which assumes a small cohesion region at the crack tip, as shown in Fig. 14, where part of the crack surface is not subjected to any force, while the part of the cohesive zone is subject to cohesive forces [77]. Therefore, the mechanical behavior of the complex deformation area near the crack tip can be described by the opening stress and displacement of the crack surface using the cohesive model, which effectively avoids the problems of traditional fracture models. The cohesive model can be used to simulate crack propagation behavior and interface problems in composite materials.

4.1.1. Cohesive model

The cohesive model describes the relationship between tension and opening displacement, distinguishing it according to its curve shape and cohesive parameters. Currently, the widely used cohesive models mainly include exponential, bilinear, polynomial, and trapezoidal models [75], as shown in Fig. 15.

Taking the bilinear cohesive model as an example, the cohesive model mainly includes the interface stiffness K, interface strength σ, and interface separation δ, as shown in Fig. 16. When $\delta = \delta_0$, the interface begins to yield; when $\delta = \delta_{max}$, the interface is completely debonded; when $\delta_0 < \delta < \delta_{max}$, there is a relationship as shown in Equation (23) [7].

$$\begin{bmatrix} \sigma_n \\ \sigma_s \\ \sigma_t \end{bmatrix} = \begin{pmatrix} (1-D)K_{nn} & & \\ & (1-D)K_{ss} & \\ & & (1-D)K_{tt} \end{pmatrix} \begin{bmatrix} \delta_n \\ \delta_s \\ \delta_t \end{bmatrix} \tag{23}$$

σ_n、 σ_s and σ_t are the normal stress and two orthogonal shear stresses, respectively. δ_n、 δ_s and δ_t are the strains in each direction. D ($0 \leq D \leq 1$) is the interfacial debonding damage coefficient, and K_{nn}、 K_{ss} and K_{tt} are the stiffness coefficients in each direction. When D is equal to 0, the interface has not been damaged and can bear the load. When D is equal to 1, the interface is completely debonded and cannot bear the load.

4.2. Methods of obtaining interface performance parameters

Although the cohesive model can describe the interface behavior of composite materials well, the cohesive model has a strong dependence on the accuracy of the interface performance parameters. Since the size of PRMMCs is in the micron range and below, it is difficult to obtain accurate interface performance parameters through conventional experimental methods due to the limitations of experimental methods and conditions [75,78].

4.2.1. Microscopic mechanical property testing

In recent years, with the development of micro/nano-scale mechanical testing technologies such as nanoindentation, atomic force microscopy, etc., it has become possible to accurately measure the microscopic mechanical properties of materials. Nanoindentation techniques [78], nano scratch techniques [78], micro-pillar compression techniques [79], and in-situ TEM tensile techniques [80], etc. Have achieved certain achievements in the interfacial mechanical property testing of PRMMCs. However, these microscopic mechanical experiments are limited by the loading conditions of experimental equipment and the complex interface shape of PRMMCs, and cannot reproduce the complex stress state of the reinforcing particles in the metal matrix, making it difficult to measure the accurate interfacial mechanical properties of PRMMCs.

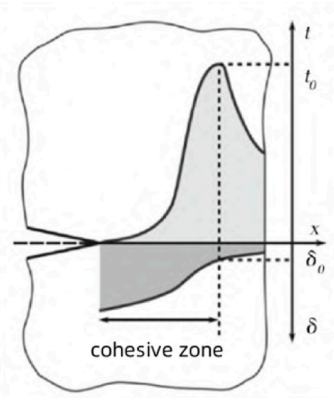

Fig. 14. The cohesive zone at the crack tip.

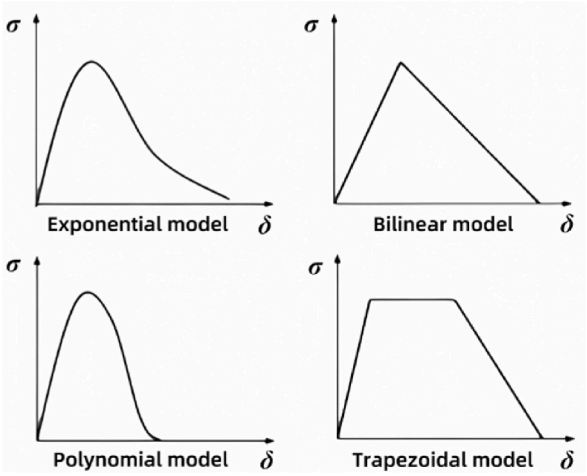

Fig. 15. Different forms of cohesive curves.

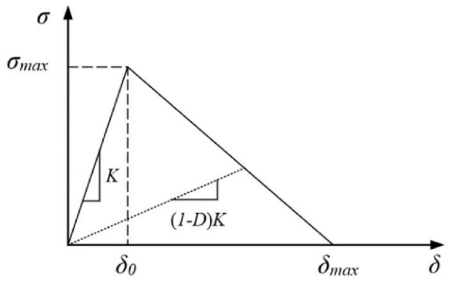

Fig. 16. Bilinear cohesive model.

4.2.2. The method of combining experiment and finite element

This method first prepares the samples of the composite material, performs tensile testing to obtain the stress-strain curve of the material, and then establishes a finite element model for simulation. Combined with the experimental data, the input parameters of the finite element model were modified to obtain the performance parameters of the composite interface. Feng et al. [81] measured the interfacial performance parameters of composite solid propellant particles/matrix by inversion method. The principle is to calculate the error between the simulation results and the experimental results through the overlap degree target function, and continuously modify the initial values of the input interface parameters of the simulation until the error is less than the selected tolerance to obtain the optimal solution of the interface mechanical properties. Fig. 17 shows the flowchart of the inversion method. Guo et al. [82] prepared PDMS-based composite samples filled with single ZrO2 spherical particles and performed uniaxial tension tests. In the initial stage of tension, as shown in Fig. 18, debonding occurred at the top and bottom vertices of the particles, can first determine the normal strength of the interface. Then build a finite element model for tensile simulation, and the interfacial stiffness K, normal strength σ_{max}, and shear strength τ_{max} were obtained by combining experimental and finite element results.

4.2.3. Molecular dynamics simulation of interface

The molecular dynamics simulation method can reveal the damage mechanism of the interface from a microscopic perspective and obtain the dynamic statistical information of the system. It simulates the interactions and movements between microscopic particles in a multi-body system at the molecular or atomic scale. The key to the accuracy of molecular dynamics results lies in the selection of the interatomic potential function [7,36,73]. The stress-strain relationship of the interface was obtained by molecular dynamics simulation, and the mechanical properties of the interface were obtained. The main steps of molecular dynamics simulation for studying the mechanical behavior of interface are.

(1) Establish a finite element model of the composite material and calculate the stress-strain at the interface;
(2) Select an appropriate potential function to establish an atomic model at the interface;
(3) Apply the stress-strain calculated by the finite element model to the boundary atoms and repeat this step until the interface fails to bear the load.

Fig. 19 (a) to (d) shows the four stages of interface debonding in molecular dynamics simulations.

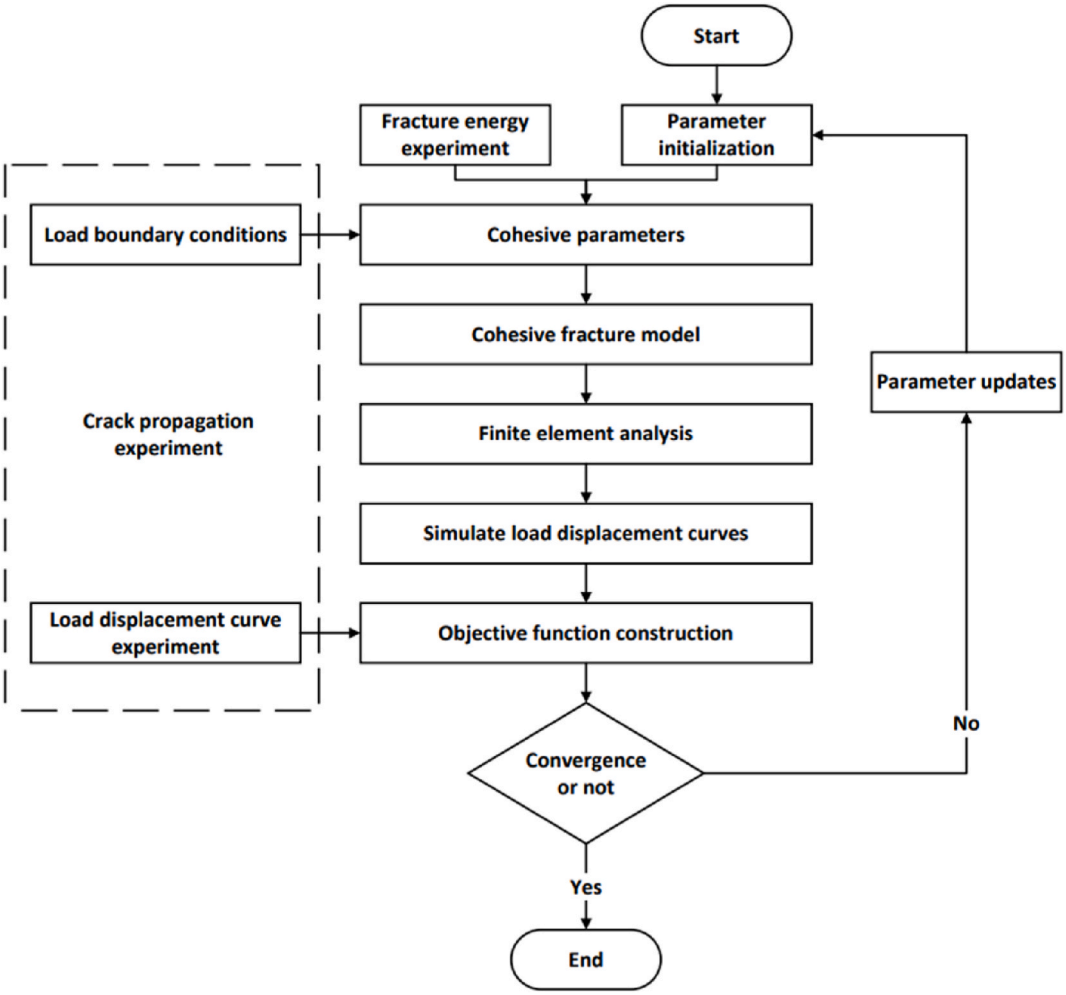

Fig. 17. Flowchart of the inversion method.

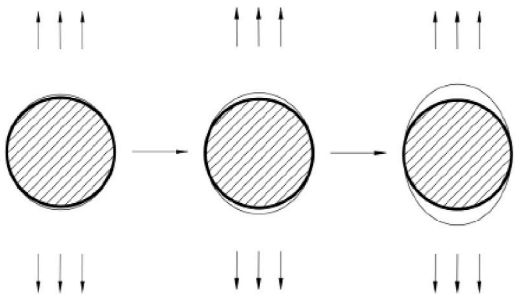

Fig. 18. Interface debonding.

Molecular dynamics simulations are influenced by the size of the model, as the more atoms included in the simulation, the more accurate the results. However, this reduces the efficiency of the calculations. Therefore, when using molecular dynamics simulations to study interface debonding, a trade-off between accuracy and efficiency is necessary. The use of periodic boundary conditions can improve this issue, but for PRMMCs with complex interface shapes, implementing periodic boundary conditions can be challenging.

5. Secondary development of Anaqus

The finite element research of PRMMCs extensively utilizes Abaqus, which offers a wide range of interfaces and supports the

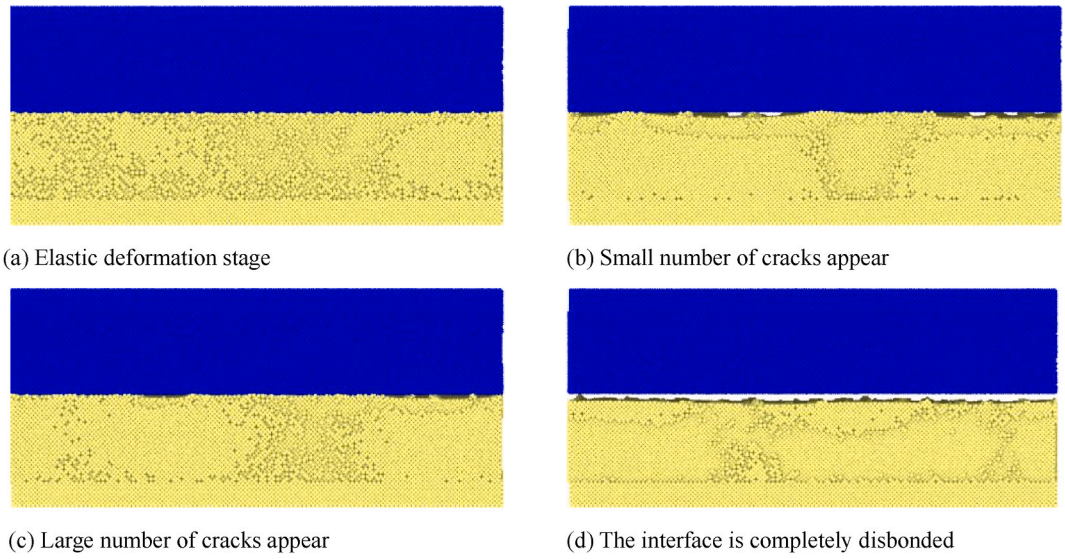

Fig. 19. Molecular dynamics simulation of interface debonding process.

importation of models in various formats. Users have the capability to generate models using third-party software, import them into Abaqus, and conduct analysis after processing. For instance, Peng et al. [14] established a B_4C_p/Al model using X-CT technology and imported it into Abaqus for simulation to study the influence of B_4C particle size on the mechanical properties of B_4C_p/Al. Similarly, Fan et al. [24] used Digimat software to establish a random distribution model of SiC_p/Al, and imported the model into Abaqus for cutting simulation to analyze the dynamic removal mechanism of materials and the formation process of cutting surface during cutting. Furthermore, parameterized modeling can be achieved through Python scripts via the secondary development interface provided by Abaqus. As an example, Lu et al. [83] used Python script to establish a 2D model of SiC_p/Al in Abaqus, and carried out cutting simulation to study the influence of tool front Angle and relative position of tool grains on SiC_p/Al precision cutting. Miao et al. [29], on the other hand, developed a three-dimensional model of ZTA_p/Fe_{45} in Abaqus using Python script for impact simulations and examined how varying ZTA particle volume fraction affects the impact toughness characteristics of ZTA_p/Fe_{45}. The rich extensibility of Abaqus makes it a powerful tool for studying PRMMCs.

The Abaqus software features a relatively straightforward built-in modeling function, complemented by a Python scripting interface that allows for script writing using the Python language, as illustrated in Fig. 20 [84,85]. To interact with the Abaqus kernel, users can utilize either the Command Line Interface (CLI) or select the "Run Script" option within the Abaqus/CAE window. In addition, several researchers have developed Python scripts that are integrated into the Abaqus main interface or offered as plug-ins [5,86]. This allows users to directly interact with Abaqus through the user interface and facilitates the construction of geometric models.

To apply the constitutive equation of metal matrix based on PRMMCs strengthening mechanism to finite element analysis, the user material subroutine interface provided by Abaqus can be used. Mathematical equations can be written as code using Fortran language, namely the user material subroutine [87]. The user material subroutine includes UMAT and VUMAT, which are applied to

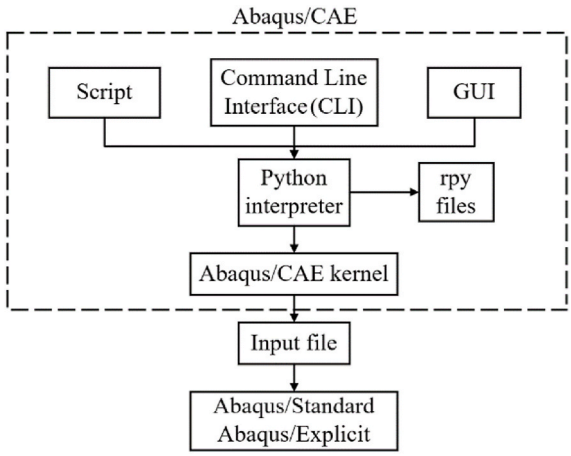

Fig. 20. The interaction mechanism of Abaqus.

Abaqus/Standard and Abaqus/Explicit, respectively. The user material subroutine communicates with Abaqus' main solver program through an interface, using the keyword "*USER MATERIAL" to define user material properties. By using the user material subroutine, materials that are not in the Abaqus material library can be defined and can be used for almost any mechanical analysis process and can be assigned to any element in Abaqus with user material properties [88,89].

There are many secondary development interfaces for Abaqus, and this section mainly introduces the construction of PRMMCs geometric models mentioned in this article and the application of constitutive equations in Abaqus.

6. Conclusion

At present, the research on the finite element modeling of PRMMCs is constantly deepening, and the accuracy and universality of the model are constantly improving. In this paper, the finite element modeling research based on the mesoscopic structure of PRMMCs is summarized, and the main conclusions are as follows：

(1) By utilizing computer parametric modeling, the input parameters can be adjusted to control the volume fraction and particle shape of the model, which exhibits a high level of universality, but this model still has certain differences from the real structure of the material. On the other hand, employing a real structure model allows for an accurate representation of the material's microstructure; nevertheless, this approach is laborious, inefficient, and the integrity of the sample cannot be preserved.
(2) PRMMCs have multiple reinforcement mechanisms, mainly aimed at strengthening the metal matrix. Among them, thermal mismatch, modulus mismatch and grain refinement play a leading role in the strengthening of the matrix, and the strengthening mechanism of PRMMCs should be considered when establishing the constitutive equation of the matrix.
(3) The behavior of the interface can be described by the cohesive model, but it has a strong dependence on interface performance parameters. Micro-mechanical performance tests, experiments combined with finite element methods, and molecular dynamics methods can obtain interface performance parameters of PRMMCs, but these methods still have shortcomings.
(4) The finite element research of PRMMCs extensively utilizes Abaqus, which provides users with many secondary development interfaces. With the help of Python script for secondary development of Abaqus, parametric modeling can be achieved in Abaqus, and material properties that are not available in the Abaqus material library can be defined through the user material subprogram interface, allowing users to apply their own constitutive equations to finite element analysis.

6.1. Scope for future work

Through research, it is found that the finite element modeling based on mesoscopic structure of PRMMCs has been relatively mature, but there are some limitations in the current method. It is difficult to consider the aggregation behavior of particles in PRMMCs by using random particle distribution in parametric modeling. The modeling process based on material slice image is complicated, and the complete sample cannot be retained. Limited by the experimental methods and conditions, it is difficult to obtain accurate material performance parameters.

Currently, with the widespread adoption of big data and the continuous enhancement of computer performance, artificial intelligence technologies such as deep learning and reinforcement learning have experienced rapid advancements and found applications across diverse research domains [7,90]. Use the actual microstructure of PRMMCs to train the neural network to construct an accurate meso-3D model of the material. The correlation between microstructure and material properties of PRMMCs is extracted through big data analysis, enabling precise prediction of the mechanical properties of materials. The utilization of artificial intelligence technology in modeling is the prevailing trend for PRMMCs meso-finite element research.

Data availability statement

This is a review paper, so all the data can be found in the article.

CRediT authorship contribution statement

Jing Li: Writing – original draft, Investigation, Formal analysis. **Fei Wang:** Writing – review & editing, Supervision, Methodology, Funding acquisition. **Ce Zhang:** Investigation. **Qifei Li:** Investigation. **Tao Chen:** Supervision, Funding acquisition.

Declaration of competing interest

The authors declare that they have no known competing financial interests or personal relationships that could have appeared to influence the work reported in this paper.

Acknowledgments

This work was supported by Natural Science Foundation of Shandong Province (No. ZR2020ME116), the Key Research and Development Program of Shandong Province (No. 2020CXGC011004), the Science, Education and Industry Integration Innovation

Pilot Project from Qilu University of Technology (Shandong Academy of Sciences) under Grant No. 2022PY005.

References

[1] H. Zhou, P. Yao, T. Gong, Y. Xiao, Z. Zhang, L. Zhao, et al., Effects of ZrO2 crystal structure on the tribological properties of copper metal matrix composites, Tribol. Int. 138 (2019) 380–391.
[2] H.A. Kishawy, A. Hosseini. Machining Difficult-to-Cut Materials, Materials Forming, Machining and Tribology, Springer International Publishing, 2019.
[3] A.K. Sharma, R. Bhandari, A. Aherwar, R. Rimašauskienė, C. Pinca-Bretotean, A study of advancement in application opportunities of aluminum metal matrix composites, Mater. Today: Proc. 26 (2020) 2419–2424.
[4] x Yu, X. Bo, Progress in the study of strengthening mechanisms of particle-reinforced metal matrix composites, Modern Manufacturing Technology and Equipment 58 (4) (2022) 98–100.
[5] Z. Xin, Numerical Simulation of the Mechanical Properties of Particle-Reinforced Metal Matrix Composites [Doctor], China University of Mining & Technology, Beijing, 2020.
[6] J. Liu, J. Zhang, C. Zhang, X. Huang, Comparison of microscopic finite element modeling methods for particle-reinforced metal matrix composites, Mater. Mech. Eng. 46 (4) (2022) 82–88, 94.
[7] Y. Yu, Y. Su, Q. Ouyang, Q. Guo, D. Zhang, Progress in the structural modeling and mechanical simulation of particle-reinforced metal matrix composites, Rare Met. Lett. 39 (3) (2020) 214–225.
[8] J. Zhou, M. Lu, J. Lin, et al., Investigation and simulation based on mesoscopic model of SiCp/Al composites during precision machining: deformation mechanism and surface quality, Int. J. Adv. Des. Manuf. Technol. (2022) 1–14.
[9] P. Zhang, X. Yue, Q. Zhang, et al., Investigation on the influence of SiC particle parameters on the machinability of SiCp/Al composite, Vacuum 191 (2021) 110340.
[10] Y. Chen, X. Zhang, Study on the cutting mechanism of SiCp/Al considering particle size and distribution, Int. J. Adv. Des. Manuf. Technol. 115 (4) (2021) 1211–1225.
[11] Y. Chen, Y. Ma, F. Pan, S. Wang, The research progress of multiscale composite mechanics, Chinese Journal of Solid Mechanics 39 (1) (2018) 1–68.
[12] Z. Lin, Y. Su, C. Qiu, J. Yang, X. Chai, X. Liu, et al., Configuration effect and mechanical behavior of particle reinforced aluminum matrix composites, Scripta Mater. 224 (2023) 115135.
[13] Q. Liu, F. Qi, Q. Wang, H. Ding, K. Chu, Y. Liu, et al., The influence of particles size and its distribution on the degree of stress concentration in particulate reinforced metal matrix composites, Mater. Sci. Eng., A 731 (2018) 351–359.
[14] P. Peng, M. Gao, E. Guo, H. Kang, H. Xie, Z. Chen, et al., Deformation behavior and damage in B4Cp/6061Al composites: an actual 3D microstructure-based modeling, Mater. Sci. Eng., A 781 (2020) 139169.
[15] G. Jagadeesh, S. Gangi Setti, A review on micromechanical methods for evaluation of mechanical behavior of particulate reinforced metal matrix composites, J. Mater. Sci. 55 (2020) 9848–9882.
[16] Y. Wang, L. Li, K. Yang, Simulation of the mechanical properties of ultra-precision cutting of SiC_p/Al composite materials, Tool Engineering 53 (4) (2019) 72–74.
[17] L. Kong, J. Wu, Simulation Study on Turning of SiCp/Al Composite Materials, Light Industry Machinery, 2021.
[18] M. Fathipour, M. Hamedi, R. Yousefi, Numerical and experimental analysis of machining of Al (20 vol% SiC) composite by the use of ABAQUS software, Mater. Werkst. 44 (1) (2013) 14–20.
[19] L. Zhou, S.T. Huang, D. Wang, X.L. Yu, Finite element and experimental studies of the cutting process of SiCp/Al composites with PCD tools, Int. J. Adv. Manuf. Technol. 52 (5–8) (2011) 619–626.
[20] P. Zhang, X. Yue, Q. Zhang, C. Zong, Y. Fang, Investigation on the influence of SiC particle parameters on the machinability of SiCp/Al composite, Vacuum 191 (5–8) (2021) 110340.
[21] X. Chen, L. Chen, H. Chen, B. Song, Y. Zhao, T. Yu, et al., Meso-scale numerical simulation and experimental verification of single grain grinding TiC–Fe composites, Ceram. Int. 48 (9) (2022) 12299–12310.
[22] W. Sun, H. Hu, B. Yu, L. Sheng, G. Hu, Y. Cai, et al., Random model for radiation shielding calculation of particle reinforced metal matrix composites and its application, Appl. Radiat. Isot. 166 (2020) 109299.
[23] W. Zhang, H. Chen, R. Prentki, Numerical analysis of the mechanical behavior of ZTAp/Fe composites, Comput. Mater. Sci. 137 (2017) 153–161.
[24] Y. Fan, Y. Xu, Z. Hao, J. Lin, Dynamic behavior description and three-dimensional cutting simulation of SiCp/Al composites with high volume fraction, J. Manuf. Process. 77 (2022) 174–189.
[25] M.D. Rintoul, S. Torquato, Reconstruction of the structure of dispersions, J. Colloid Interface Sci. 186 (2) (1997) 467–476.
[26] D.-W. Kim, J.H. Lim, J. Yu, Efficient prediction of the electrical conductivity and percolation threshold of nanocomposite containing spherical particles with three-dimensional random representative volume elements by random filler removal, Compos. B Eng. 168 (2019) 387–397.
[27] T. Vaughan, C. McCarthy, A combined experimental–numerical approach for generating statistically equivalent fibre distributions for high strength laminated composite materials, Compos. Sci. Technol. 70 (2) (2010) 291–297.
[28] W. Wang, Y. Dai, C. Zhang, X. Gao, M. Zhao, Micromechanical modeling of fiber-reinforced composites with statistically equivalent random fiber distribution, Materials 9 (8) (2016) 624.
[29] L. Yang, Y. Yan, Z. Ran, Y. Liu, A new method for generating random fibre distributions for fibre reinforced composites, Compos. Sci. Technol. 76 (2013) 14–20.
[30] Y. Ismail, D. Yang, J. Ye, Discrete element method for generating random fibre distributions in micromechanical models of fibre reinforced composite laminates, Compos. B Eng. 90 (2016) 485–492.
[31] W. Miao, Z. Xin, Y. Qin, Y. Wang, H. Chen, Dynamic modeling of particle reinforced composites and its Charpy impact test verification, Mater. Today Commun. 30 (2022) 103040.
[32] W. Cheng, Research on the method of generating a three-dimensional random convex aggregate model of concrete, J. Hydraul. Eng. 42 (5) (2011) 609–615.
[33] Y. Su, Q. Ouyang, W. Zhang, Z. Li, Q. Guo, G. Fan, et al., Composite structure modeling and mechanical behavior of particle reinforced metal matrix composites, Mater. Sci. Eng., A 597 (2014) 359–369.
[34] Q. Wu, L. Zhang, Microstructure-based three-dimensional characterization of chip formation and surface generation in the machining of particulate-reinforced metal matrix composites, Int. J. Extrem. Manuf. 2 (4) (2020) 045103.
[35] B. Wang, H. Wang, Z. Zhang, M. Zhou, Research on microstructure modeling method of three-dimensional random rough aggregates in concrete, Chin. J. Appl. Mech. 35 (5) (2018) 1072–1076.
[36] J. Xiang, Non-continuity of the Dynamic Mechanical Behavior and Cutting Performance Study of SICP/Al Composite Materials, Beijing Institute of Technology, 2018.
[37] M. Gao, Z. Chen, H. Kang, E. Guo, R. Li, Y. Fu, et al., Microstructural characteristics and mechanical behavior of B4Cp/6061Al composites synthesized at different hot-pressing temperatures, J. Mater. Sci. Technol. 35 (8) (2019) 1523–1531.
[38] M.P. Echlin, T.L. Burnett, A.T. Polonsky, T.M. Pollock, P.J. Withers, Serial sectioning in the SEM for three dimensional materials science, Curr. Opin. Solid State Mater. Sci. 24 (2) (2020) 100817.
[39] N. Chawla, K. Chawla, Microstructure-based modeling of the deformation behavior of particle reinforced metal matrix composites, J. Mater. Sci. 41 (2006) 913–925.
[40] J. Xiang, L. Xie, F. Gao, J. Yi, S. Pang, X. Wang, Methodology for dependence-based integrated constitutive modelling: an illustrative application to SiCp/Al composites, Ceram. Int. 44 (10) (2018) 11765–11777.

[41] G.R. Johnson, A constitutive model and data for materials subjected to large strains, high strain rates, and high temperatures, in: Proc 7th Inf Sympo Ballistics, 1983, pp. 541–547.
[42] S. Li, B. Hou, Material behavior modeling in machining simulation of 7075-T651 aluminum alloy, J. Eng. Mater. Technol. 136 (1) (2014).
[43] W. Song, J. Ning, X. Mao, H. Tang, A modified Johnson–Cook model for titanium matrix composites reinforced with titanium carbide particles at elevated temperatures, Mater. Sci. Eng., A 576 (2013) 280–289.
[44] M. Calamaz, D. Coupard, F. Girot, A new material model for 2D numerical simulation of serrated chip formation when machining titanium alloy Ti–6Al–4V, Int. J. Mach. Tool Manufact. 48 (3–4) (2008) 275–288.
[45] T. Özel, M. Sima, A. Srivastava, B. Kaftanoglu, Investigations on the effects of multi-layered coated inserts in machining Ti–6Al–4V alloy with experiments and finite element simulations, CIRP annals 59 (1) (2010) 77–82.
[46] D. Umbrello, S. Rizzuti, J. Outeiro, R. Shivpuri, R. M'Saoubi, Hardness-based flow stress for numerical simulation of hard machining AISI H13 tool steel, J. Mater. Process. Technol. 199 (1–3) (2008) 64–73.
[47] S. Nemat-Nasser, J. Isaacs, Direct measurement of isothermal flow stress of metals at elevated temperatures and high strain rates with application to Ta and TaW alloys, Acta Mater. 45 (3) (1997) 907–919.
[48] G.R. Johnson, T.J. Holmquist, Response of boron carbide subjected to large strains, high strain rates, and high pressures, J. Appl. Phys. 85 (12) (1999) 8060–8073.
[49] T. Holmquist, G. Johnson, Response of boron carbide subjected to high-velocity impact, Int. J. Impact Eng. 35 (8) (2008) 742–752.
[50] R. Li, Q. Yao, M. Liu, G. Gao, D. Jiang, Study on the resistance of close-range explosion analysis of nuclear power plant safety containment structure based on ABAQUS platform JH-2 constitutive model, Building Structure 52 (S1) (2022) 431–435.
[51] P. Xu, S. Zuo, Study on the JH-2 model parameters for metro shield cutting reinforced concrete pile, Geotech. Geol. Eng. 39 (2021) 5267–5278.
[52] C. Oucif, L.M. Mauludin, Numerical modeling of high velocity impact applied to reinforced concrete panel, Undergr. Space 4 (1) (2019) 1–9.
[53] K. Bao, X. Zhang, M. Tan, B. Chen, H. Wei, Experimental and numerical simulation study on bullet impact of boron carbide ceramic composite target, Explos. Shock Waves 39 (12) (2019) 54–65.
[54] J. Zhang, H. Andrae, X. Zhang, Q. Wang, B. Xiao, Z. Ma, An enhanced finite element model considering multi strengthening and damage mechanisms in particle reinforced metal matrix composites, Compos. Struct. 226 (2019) 111281.
[55] A. Sanaty-Zadeh, Comparison between current models for the strength of particulate-reinforced metal matrix nanocomposites with emphasis on consideration of Hall–Petch effect, Mater. Sci. Eng., A 531 (2012) 112–118.
[56] N. Ramakrishnan, An analytical study on strengthening of particulate reinforced metal matrix composites, Acta Mater. 44 (1) (1996) 69–77.
[57] L. Cheng, W. Poole, J. Embury, D. Lloyd, The influence of precipitation on the work-hardening behavior of the aluminum alloys AA6111 and AA7030, Metall. Mater. Trans. 34 (2003) 2473–2481.
[58] A.P. Reddy, P.V. Krishna, R. Rao, Mechanical and wear properties of aluminum-based nanocomposites fabricated through ultrasonic assisted stir casting, J. Test. Eval. 48 (4) (2018) 3035–3056.
[59] Y. Wu, E. Lavernia, Strengthening behavior of particulate reinforced MMCs, Scripta Metall. Mater. 27 (2) (1992) 173–178.
[60] W. Miller, F. Humphreys, Strengthening mechanisms in particulate metal matrix composites, Scripta Metall. Mater. 25 (1) (1991) 33–38.
[61] C. Wu, K. Ma, J. Wu, P. Fang, G. Luo, F. Chen, et al., Influence of particle size and spatial distribution of B4C reinforcement on the microstructure and mechanical behavior of precipitation strengthened Al alloy matrix composites, Mater. Sci. Eng., A 675 (2016) 421–430.
[62] M.J.N. Isfahani, F. Payami, M.A. Asadabad, A.A. Shokri, Investigation of the effect of boron carbide nanoparticles on the structural, electrical and mechanical properties of Al-B4C nanocomposites, J. Alloys Compd. 797 (2019) 1348–1358.
[63] E. Huskins, B. Cao, K. Ramesh, Strengthening mechanisms in an Al–Mg alloy, Mater. Sci. Eng., A 527 (6) (2010) 1292–1298.
[64] E. Orowan, Discussion in the symposium on internal stresses in metals and alloys, inst, Metals, London (1948) 451.
[65] x Ye, Y. Li, J. Ong, L. Cai, C. Liu, Research status of strengthening mechanism of particle-reinforced metal matrix composites, J. Mater. Eng. 46 (12) (2018) 28–37.
[66] M. Alizadeh, Strengthening mechanisms in particulate Al/B4C composites produced by repeated roll bonding process, J. Alloys Compd. 509 (5) (2011) 2243–2247.
[67] Y. Huang, S. Qu, K. Hwang, M. Li, H. Gao, A conventional theory of mechanism-based strain gradient plasticity, Int. J. Plast. 20 (4–5) (2004) 753–782.
[68] S. Ma, X. Zhuang, X. Wang, Particle distribution-dependent micromechanical simulation on mechanical properties and damage behaviors of particle reinforced metal matrix composites, J. Mater. Sci. 56 (2021) 6780–6798.
[69] S. Shibata, M. Taya, T. Mori, T. Mura, Dislocation punching from spherical inclusions in a metal matrix composite, Acta Metall. Mater. 40 (11) (1992) 3141–3148.
[70] H. Gao, Y. Huang, Taylor-based nonlocal theory of plasticity, Int. J. Solid Struct. 38 (15) (2001) 2615–2637.
[71] H.-Y. Yang, Z. Wang, L.-Y. Chen, S.-L. Shu, F. Qiu, L.-C. Zhang, Interface formation and bonding control in high-volume-fraction (TiC+ TiB2)/Al composites and their roles in enhancing properties, Compos. B Eng. 209 (2021) 108605.
[72] T. Han, E. Liu, J. Li, N. Zhao, C. He, A bottom-up strategy toward metal nano-particles modified graphene nanoplates for fabricating aluminum matrix composites and interface study, J. Mater. Sci. Technol. 46 (2020) 21–32.
[73] X. Tang, J. Zhang, T. Ma, Research progress on interfacial microstructure and properties of particle-reinforced metal matrix composites, China Surface Engineering 35 (3) (2022) 16–30.
[74] K. Bai, S. Zhan, P. Zhang, Z. Tan, Q. Zong, Mechanics 2006-2015: situation and prospect, Advances in Mechanics 49 (1) (2019) 201911.
[75] Z. Zhang, Y. Pan, T. Zhang, X. Fu, Research progress on interface and cohesive model of metal matrix composites, Aerospace Materials & Technology 52 (3) (2022) 1–11.
[76] G.I. Barenblatt, The mathematical theory of equilibrium cracks in brittle fracture, Adv. Appl. Mech. 7 (1962) 55–129.
[77] S. Roth, G. Hütter, M. Kuna, Simulation of fatigue crack growth with a cyclic cohesive zone model, Int. J. Fract. 188 (1) (2014) 23–45.
[78] X. Guo, Q. Guo, J. Nie, Z. Liu, Z. Li, G. Fan, et al., Particle size effect on the interfacial properties of SiC particle-reinforced Al-Cu-Mg composites, Mater. Sci. Eng., A 711 (2018) 643–649.
[79] Q. Guo, Y. Han, D. Zhang, Interface-dominated mechanical behavior in advanced metal matrix composites, Nano Materials Science 2 (1) (2020) 66–71.
[80] L. Jiang, T. Hu, H. Yang, D. Zhang, T. Topping, E.J. Lavernia, et al., Deformation of a ceramic/metal interface at the nanoscale, Nanoscale 8 (20) (2016) 10541–10547.
[81] T. Feng, J. Xu, X. Chen, C. Zhou, Inversion optimization of composite solid propellant granule/matrix interface parameters, Comput. Simulat. 35 (9) (2018) 25–30.
[82] X. Guo, Y. Yao, S. Chen, A new method for predicting the interfacial mechanical properties of particle-reinforced composites, Chin. J. Theor. Appl. Mech. 53 (5) (2021) 1334–1344.
[83] S. Lu, Z. Li, J. Zhang, C. Zhang, G. Li, H. Zhang, et al., Coupled effect of tool geometry and tool-particle position on diamond cutting of SiCp/Al, J. Mater. Process. Technol. 303 (2022), 303-.
[84] Y. Qin, L. Chen, Application of ABAQUS pretreatment secondary development in parametric modeling of cutting process, Machine Tool & Hydraulics 45 (13) (2017) 4.
[85] C. Wu, C. Qi, J. Yang, N. Zhang, Application of ABAQUS secondary development in milling deformation prediction of train thin-walled frame parts, Tool Engineering 57 (3) (2023) 105–110.
[86] Tian Y., Python based Abaqus pre - and post-processing GUI plug-in secondary development and application, Comput. Aided Eng. 31 (02) (2022) 63-68.
[87] S. Hou, Secondary Development of Damage Constitutive Model of White Sandstone Based on ABAQUS [Doctor], Qingdao University of Science and Technology, Qingdao, 2022.

[88] W. Wang, Secondary Development and Application of Concrete Damage Constitutive Model Based on ABAQUS [postgraduate], North China University of Water Resources and Electric Power, 2021.
[89] Q. Wang, K. Chang, K. Hou, T. Lu, L. Liu, Concrete uniaxial constitutive model for ABAQUS beam elements, Journal of Architecture and Civil Engineering 35 (5) (2018) 194–202.
[90] J. Zhang, W. Yang, Y. Li, Application of artificial intelligence in the research of composite materials, Advances in Mechanics 4 (2021) 51.